NANO · MICRO small
www.small-journal.com

Aurozyme: A Revolutionary Nanozyme in Colitis, Switching Peroxidase-Like to Catalase-Like Activity

*Hyung Shik Kim, Sieun Lee, and Dong Yun Lee**

A therapeutic strategy that could address colitis of multiple etiologies while restoring the dysbiosis of gut microbiota is attractive. Here, Aurozyme, a novel nanomedicine comprised of gold nanoparticles (AuNPs) and glycyrrhizin (GL) with a glycol chitosan coating layer, as a promising approach for colitis, is demonstrated. The unique feature of Aurozyme is the conversion of harmful peroxidase-like activity of AuNPs to beneficial catalase-like activity due to the amine-rich environment provided by the glycol chitosan. This conversion process enables Aurozyme to oxidize the hydroxyl radicals derived from AuNP, producing water and oxygen molecules. In fact, Aurozyme effectively scavenges reactive oxygen/reactive nitrogen species (ROS/RNS) and damage-associated molecular patterns (DAMPs), which can attenuate the M1 polarization of macrophage. It exhibits prolonged adhesion to the lesion site, promoting sustained anti-inflammatory effects and restoring intestinal function in colitis-challenged mice. Additionally, it increases the abundance and diversity of beneficial probiotics, which are essential for maintaining microbial homeostasis in the gut. The work highlights the transformative potential of nanozymes for the comprehensive treatment of inflammatory disease and represents an innovative switching technology of enzyme-like activity by Aurozyme.

1. Introduction

Inflammatory bowel disease (IBD) is an intractable chronic disease instigated by multiple factors such as disrupted intestinal barrier functions, elevated levels of reactive oxygen species/reactive nitrogen species (ROS/RNS), and damage-associated molecular patterns (DAMPs), etc.[1] These hazard signals dysregulate mucosal immune responses, triggering pro-inflammatory cascades that disrupts gut microbial homeostasis and accelerates the severity of colitis.[2] Existing interventions for IBD have primarily focused on managing the disease by suppressing the immune response, but the symptoms have not been fully resolved due to the complexity of the inflammatory microenvironment.[3] Long-term use of conventional immunomodulating drugs based on small molecules or biologics can lead to serious complications.[4] To address these unmet medical challenges, we have exploited nanozyme with multiple enzyme-like activities, such as superoxide dismutase (SOD), peroxidase, and catalase involved in scavenging multiple danger signals from the microenvironment of IBD.

The exploitation of nanozymes in inflammatory disease has received tremendous attention due to their robustness in removing oxidative stress in the inflamed microenvironment.[5,6] In the past few decades, nanomaterials including carbon-based,[7] metal oxides or sulfide,[8,9] and single metal atoms[10,11] have been found to exert catalytic activities.[12] Although it generally decomposes hydrogen peroxide (H_2O_2) into hydroxyl radicals (•OH) through peroxidase-like activity, which causes detrimental to biological systems.[13,14] Recent advances have provided several techniques to mitigate the inherent peroxidase-like activity by decorating with coating molecules but in the case of gold nanoparticles (AuNP), only strategies with highly toxic mercury ions have been suggested.[15] In this study, we present a novel finding that AuNP coated with amine-rich glycol chitosan (Glycol chitosan@AuNP) has catalase-like activity with remarkable efficacy while retaining their SOD-like activity and eliminating peroxidase-like activity. As evidence, Glycol chitosan@AuNP converted ROS (such as superoxide radical ion ($O_2^{\bullet-}$), H_2O_2, and •OH) into water and oxygen molecules (**Figure 1**a). This consequence was attributed to primary and secondary amine oxidation of glycol chitosan coated onto the surface of the AuNP, which suppresses the •OH, a critical mediator for the peroxidase-like activity.

There is growing evidence for a prominent contribution of the high-mobility group box 1 protein (HMGB1), which is considered as a representative DAMP molecule that is commonly released

H. S. Kim, S. Lee, D. Y. Lee
Department of Bioengineering
College of Engineering, and BK FOUR Biopharmaceutical Innovation Leader for Education and Research Group
Hanyang University
Seoul 04763, Republic of Korea
E-mail: dongyunlee@hanyang.ac.kr
D. Y. Lee
Institute of Nano Science and Technology (INST)
Hanyang University
Seoul 04763, Republic of Korea
D. Y. Lee
Institute for Bioengineering and Biopharmaceutical Research (IBBR)
Hanyang University
Seoul 04763, Republic of Korea
D. Y. Lee
Elixir Pharmatech Inc.
Seoul 07463, Republic of Korea

The ORCID identification number(s) for the author(s) of this article can be found under https://doi.org/10.1002/smll.202302331

DOI: 10.1002/smll.202302331

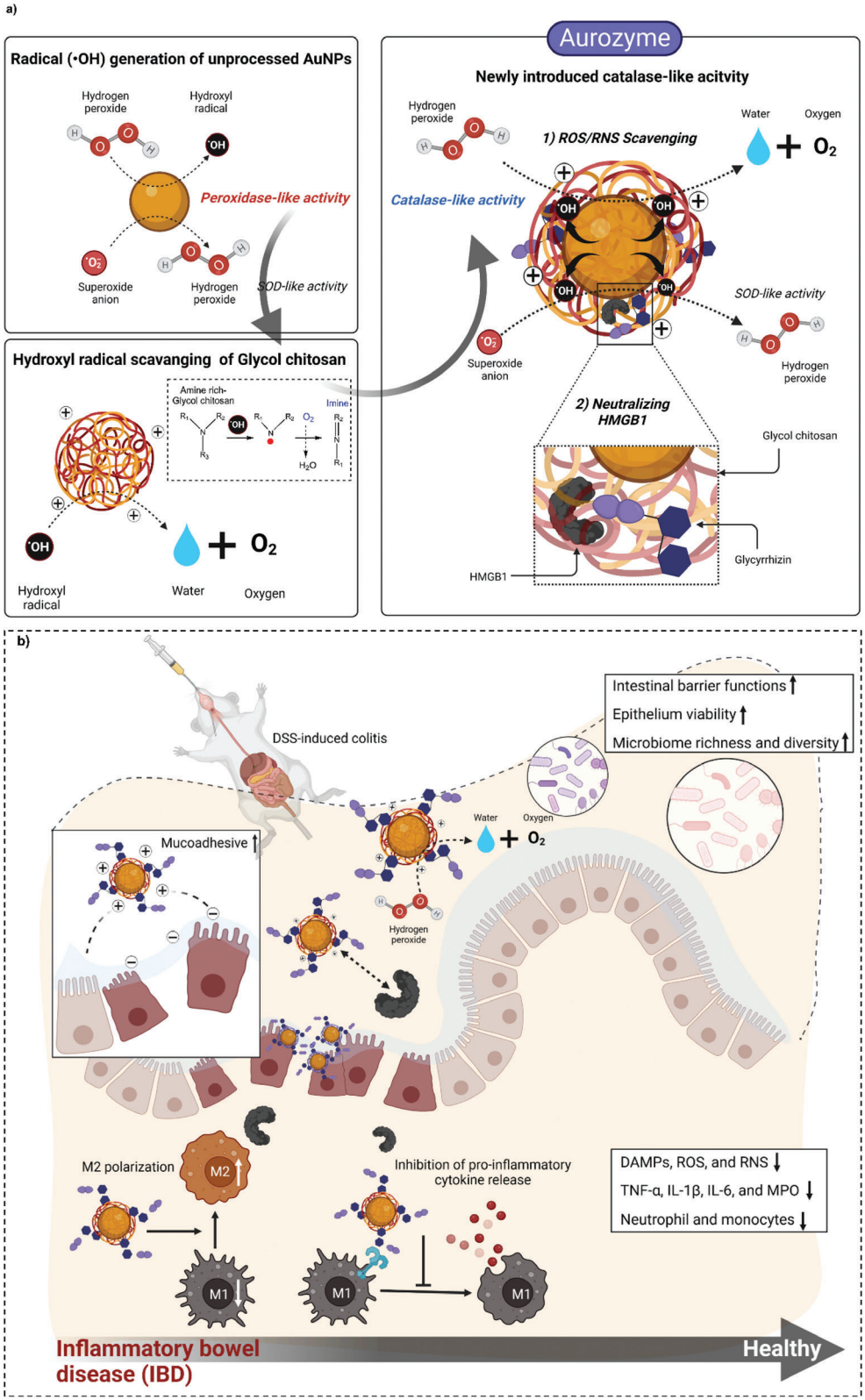

Figure 1. Schematic illustration of Aurozyme with newly introduced catalase-like activity for ROS/RNS scavenging and HMGB1 neutralization in the colitis environment. a) Schematic diagram of Aurozyme illustrating the role of glycol chitosan in converting detrimental peroxidase-like activity to beneficial catalase-like activity, and multiscavenging nanozyme against ROS/RNS and HMGB1. b) Schematic diagram of mucoadhesive Aurozyme that regulates intestinal inflammation and microflora homeostasis in colitis-challenged mice.

upon intestinal barrier disruption or secreted from activated immune cells, as a distinct stimulus to amplify inflammation in IBD.[16] Immunopathological studies of IBD also show that excessive ROS/RNS and HMGB1 generated in IBD induce a vicious self-perpetuating cycle, exacerbating pathogenesis.[17] Our hypothesis for IBD treatment: a combinatorial strategy to eliminate pro-inflammatory factors (ROS/RNS and HMGB1) would be beneficial. The anti-inflammatory glycyrrhizin (GL)[18] was further grafted to constitute a potent final formulation of gold-based nanozyme platform, i.e., Aurozyme (Figure 1a). HMGB1 neutralization and ROS/RNS scavenging in IBD lesions were achieved over a long period of time due to the mucoadhesive properties conferred by glycol chitosan. Therefore, the orally administered Aurozyme restored the tight junction and function of the intestinal barrier in the dextran sulfate sodium (DSS)-induced colitis animal model. Aurozyme regulated the imbalanced gut microbiome and promoted an abundance of beneficial bacteria that aid recovery from IBD (Figure 1b). Collectively, our study provides Aurozyme, a multiscavenging nanozyme, as a potential treatment for coping with colitis of multiple etiologies.

2. Results

2.1. Synthesis and Characterization of Surface-Coated AuNPs

We sought to investigate the enzyme-like activities of AuNP-based nanozyme toward $O_2^{\bullet}$-, H_2O_2, and •OH radicals. To this end, several materials were coated on the AuNP surface, including Citrate@AuNP, Alginate@AuNP, and Glycol chitosan@AuNP (Table S1, Supporting Information). Surface coating of AuNPs with materials did not significantly affect the colloidal stability and crystalline nature, as shown in the UV–visible spectra and X-ray powder diffraction (XRD) patterns (Figure S1, Supporting Information).[19][20] Surface-coated AuNPs (diameter 10–30 nm) were identified as spheres with a surface charge dependent on the charge of coating material (**Figure 2**a,b). Under the exposed pH conditions after oral administration, the colloidal stability of Citrate@AuNP and Alginate@AuNP was 1 h in pH 2, whereas Glycol chitosan@AuNP and Aurozyme were maintained for 3 h as shown by SPR peak and surface charge transfer (Figure S2a–S2d and Table S2, Supporting Information). This is because the cations present in the acidic solution protonate carboxylic acid of citrate and alginate and neutralize the surface charge, which in turn induces irreversible aggregation of AuNP.[21,22] On the other hand, amine-rich-glycol chitosan could circumvent aggregation. The titration-induced modulation of surface charge revealed that Citrate@AuNP and Alginate@AuNP exhibited isoelectric points at approximately pH 2 and pH 6, respectively (Figure S2e, Supporting Information). Conversely, Glycol chitosan@AuNP and Aurozyme maintained a positive surface charge throughout the entire pH range of 2–10. This result is particularly significant when considering the oral administration route, as the pH conditions of the stomach and intestine remain at pH 2 and pH 6, respectively. Consequently, Citrate@AuNP and Alginate@AuNP are susceptible to aggregation under these conditions.

2.2. Disparate Enzyme-Like Activities According to the Coating Materials on the AuNP

The scavenging activity of surface-coated AuNPs against $O_2^{\bullet}-$, H_2O_2, and •OH was investigated (Figure 2c). The SOD-like activity for $O_2^{\bullet}-$ elimination was investigated by the electron spin resonance (ESR) spectroscopy. In the reaction system in which $O_2^{\bullet}-$ was generated through xanthine/xanthine oxidase, the surface-coated AuNP effectively scavenged and diminished the signal, serving as alternative SOD mimetics (Figure 2d). The potential of surface-coated AuNPs for H_2O_2 consumption using 3,3′,5,5′-tetramethylbenzidine (TMB) and horseradish peroxidase (HRP) substrate was also investigated. This is because H_2O_2 decomposition by the peroxidase-like activity of nanozymes produces •OH, which oxidizes TMB to give a blue-color intermediate or a yellow-color end product (Figure S3, Supporting Information).[23] HRP served as a positive control and produced a distinct yellow TMB at pH 5.8. Citrate@AuNP and Alginate@AuNP showed moderate color changes of a similar magnitude (Figure 2e). Interestingly, Glycol chitosan@AuNP showed minimal activity in catalyzing TMB substrate, indicating a loss of intrinsic peroxidase-like activity and inability to oxidize the peroxidase substrate using H_2O_2.[24] The hypothesis that H_2O_2 depletion would occur due to catalase-like activity was evaluated by incubating surface-coated AuNPs with TMB in the H_2O_2 solution for 5 min, followed by HRP addition to measure H_2O_2 exhaustion through catalase-like activity. As a result, Citrate@AuNP and Alginate@AuNP immediately changed TMB to yellow before adding HRP, whereas Glycol chitosan@AuNP maintained TMB colorless even after adding HRP (Figure 2f).

2.3. Mechanism of the Catalase-Like Activity of Glycol Chitosan@AuNP

To corroborate the catalase-like activity of Glycol chitosan@AuNP, dioxygen bubble formation was observed by adding catalase (control group) or Glycol chitosan@AuNP to H_2O_2 solution (Figure 2g). Visible bubbles in the H_2O_2 solution containing the Glycol chitosan@AuNP indicate the H_2O_2 was decomposed into oxygen and water, which is a hallmark of catalase-like activity. Glycol chitosan@AuNP exhibits catalase-like activity due to its ability to scavenge •OH radicals. This is because the amine-rich structure of glycol chitosan can potentially trap the highly reactive •OH generated by the Fenton reaction from AuNPs and scavenge it through amine oxidation (Figures S4 and S5, Supporting Information).[25] The aforementioned mechanism can be attributed to the initial step in the oxidation of aliphatic amines by •OH radicals. Specifically, this route involves the loss of an alkyl group from the nitrogen atom, which results in the formation of nitramine, nitrosamine, or imines.[26] It is believed that imines, in turn, undergo reactions that ultimately lead to the formation of aldehyde products. Consistently, both Glycol chitosan and Chitosan oligosaccharide (COS) generated dioxygen bubbles in a solution containing •OH (Figure 2h,i), suggesting no dependence on the molecular weight of chitosan. The results of ^{1}H NMR also showed the product of hydroxylamine around 6.5–7.2 ppm after oxidation with •OH (Figure 2j).

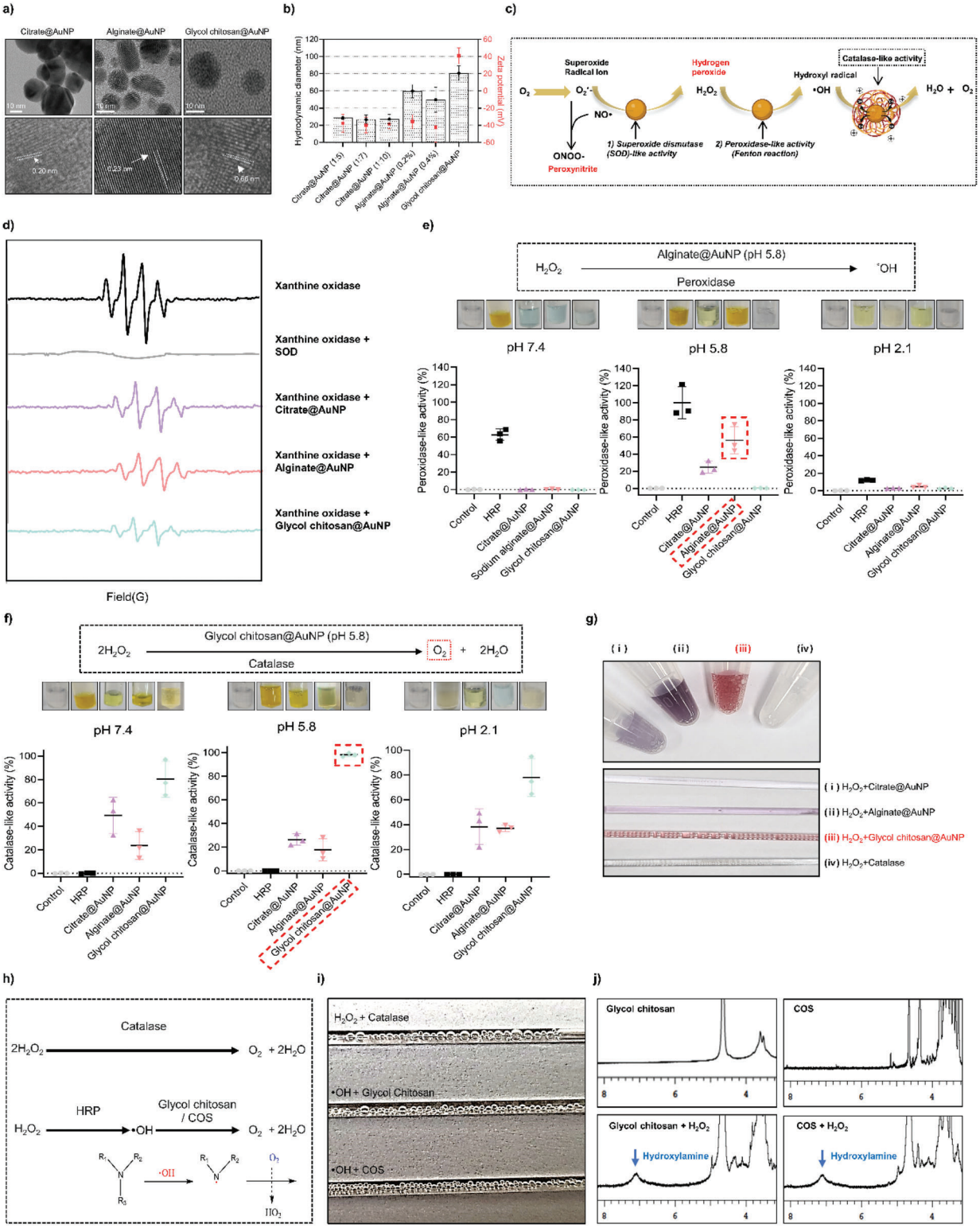

Figure 2. ROS scavenging via the catalase-like activity of Glycol chitosan@AuNP. a) TEM images and lattice parameters of Citrate@AuNP, Alginate@AuNP, and Glycol chitosan@AuNP. Scale bar: 10 nm. b) Hydrodynamic diameter (DLS) and surface charge (zeta potential) of coated AuNP, respectively. Data are expressed as mean ± SEM ($n = 3$). c) Schematic diagram of multiple enzyme-like activities of surface-coated AuNP. d) ESR spectrum results to verify superoxide dismutase (SOD)-like activity. e) Examination of the peroxidase-like activity of surface-coated AuNPs: To confirm the peroxidase-like activity, surface-coated AuNPs (125 μg mL^{-1}) were added to the reaction solution of TMB and H_2O_2 (80×10^{-3} M, adjusted to pH 7.4, 5.8, and 2.1, respectively) and reacted for 5 min. HRP (1000 IU mL^{-1}) was reacted with reaction solution (TMB and H_2O_2) for 5 min to serve as a positive control. Results of peroxidase-like activity (%) were normalized based on HRP activity at pH 5.8. Data are expressed as mean ± SEM ($n = 3$). f)

2.4. Restoration of Intestinal Barrier Functions via ROS/RNS Scavenging

The effect of surface-coated AuNPs on cell viability was evaluated and found to be no impairments at concentrations of 7.8–125 μg mL^{-1} (Figure S6, Supporting Information). The antioxidant properties were investigated by 2,2′-azino-bis (3-ethylbenzothiazoline 6-sulfonate) (ABTS) analysis. Among them, Glycol chitosan@AuNP showed the highest performance (**Figure 3**a). Intracellular ROS and nitric oxide (•NO) were detected by 2′,7′-dichlorofluorescin diacetate (DCF-DA) fluorescence assay in intestinal Caco-2 cells after H_2O_2 stimulation (Figure 3b,c).[27] 4-h treatment with H_2O_2 increased intracellular DCF fluorescence, but its level was downregulated due to its ROS/RNS scavenging effect. From a chemical point of view, the reaction between •NO and thiol-rich AuNPs produces the free radical adduct Au-S-N-HO•, which reacts with a second •NO molecule to form nitroxyl (HNO) and a nitrosothiol-Au (Au-S-N=O). The intermediate Au-S-N=O then reacts with Au-SH to form a second molecule of HNO and Au-S-S-Au (Figure S7, Supporting Information). Such a series of processes eliminate biohazardous •NO by reconstitution into HNO, which has a short half-life and is not considered as RNS.[28] Apart from the •NO, the scavenging capability of surface-coated AuNPs for nitrite (NO_2^-) in the lipopolysaccharide (LPS)-stimulated RAW 264.7 macrophages was explored,[29] and all of them scavenged ≈50% amount of NO_2^- (Figure 3d). Multiple ROS/RNS scavenging is expected to invigorate restoration of intestinal barrier function due to their mutually synergistic relationship in the IBD.[30] Overload-induced oxidative stress can damage extracellular and tight junction proteins by producing free radicals and nitrogen dioxide (NO_2•) by causing protonation of homogeneous fission.[31,32] Therefore, tight junction recovery for H_2O_2-stimulated Caco-2 cell were investigated. Figure 3e demonstrates that oxidative stress destructs tight junction proteins, whereas treatment of the surface-coated AuNPs recovered them (Figure S8, Supporting Information).

2.5. Suppression of M1 Polarization and Proinflammatory Cytokine Release

Flow cytometry was employed to investigate the effect of Alginate@AuNP and Glycol chitosan@AuNP on M1/M2 macrophage polarization. LPS stimulation evoked the M1 polarization ($CD80^+$ $CD206^-$), but treatment with Alginate@AuNP and Glycol chitosan@AuNP gradually reduced their populations (**Figure 4**a,b). Conversely, M2-positive macrophages further increased in direct proportion to the M1 reduction. In a study of macrophages stained with inducible nitric oxygen synthase (iNOS)/CD163, the M1 population increased by 12.8% upon LPS stimulation and decreased to 7.41% and 4.03% after treatments (Figure 4c,d). Pseudopodia expansion in M1-polarized cells began to be detected after 4 h and expanded at 18 h, but Alginate@AuNP or Glycol chitosan@AuNP suppressed their transformation (Figure 4e). Reflecting the inhibition of macrophage M1 polarization and promotion of M2 polarization, the proinflammatory cytokines were measured. LPS treatment upregulated tumor necrosis factor-alpha (TNF-α), interleukin-6 (IL-6), interleukine-1β (IL-1β), iNOS, and monocyte chemoattractant protein-1 (MCP-1) in both mRNA and protein level (Figure 4f,g). Alginate@AuNP provided a marginal benefit, whereas Glycol chitosan@AuNP showed a significant benefit, indicating that the catalase-like activity mitigates the inflammatory response more effectively than the peroxidase-like activity.

2.6. Aurozyme, a Multihazard Signals (ROS/RNS and HMGB1) Scavenger in the Colitis Microenvironment

For the development of more advanced therapeutic nanozymes, we further grafted glycyrrhizin (GL), which has been demonstrated as an inhibitor of HMGB1 involved in the inflammatory response (denoted as "Aurozyme"). The synthetic process was detailed in Figures S9 and S10 (Supporting Information) and confirmed by ^{1}H NMR and Fourier-transform infrared (FT-IR) (Figures S11–S14, Supporting Information). Colitis microenvironment was created by coculturing Caco-2 and RAW 246.7 cells in the trans-well culture system (Figure 4h) and induced intestinal barrier damage of Caco-2 cells by treating with H_2O_2 (Figure S15, Supporting Information), which led to the release of HMGB1 into the basolateral side. The release of HMGB1 could stimulate the RAW 246.7 macrophage in the basolateral side, thereby inducing their M1 polarization. In fact, H_2O_2 treatment increased HMGB1 concentration in the basolateral side, while Aurozyme very significantly reduced it through GL action (Figure 4i). Both Glycol chitosan@AuNP and Aurozyme reduced M1 polarization after $H_2O_2^-$ induced damage, and their morphological investigations were consistent (Figure 4j,k). Interestingly, Glycol chitosan@AuNP showed 53.16% promotion of M2 polarization, whereas Aurozyme had no significant effect (Figure 4k,l). This could be explained by the colligation of ROS/RNS and HMGB1 scavenging capability by Aurozyme does not stimulate monocyte to differentiate into inflammatory subsets in this corresponding colitis model. As evidenced, the secretion of proinflammatory cytokines from macrophages activated by HMGB1 was barely detected in the Aurozyme treatment (Figure 4m). Taken

Examination of catalase-like activity of surface-coated AuNPs. Solutions containing H_2O_2 (80×10^{-3} M), TMB, and surface-coated AuNPs (125 μg mL^{-1}) were reacted at pH 7.4, 5.8, and 2.1 for 5 min, respectively. Afterward, HRP solution (1000 IU mL^{-1}) was further added to detect the remaining H_2O_2. The catalase-like activity was normalized based on Glycol chitosan@AuNP activity at pH 5.8. Data are expressed as mean ± SEM ($n = 3$). g) Observation of the dioxygen bubbles generated at 5 min in H_2O_2 (80×10^{-3} M) solution with i) Citrate@AuNP (125 μg mL^{-1}), ii) Alginate@AuNP (125 μg mL^{-1}), iii) Glycol chitosan@AuNP (125 μg mL^{-1}), and iv) catalase. h) Equation of dioxygen bubbling by the enzymatic reaction by Catalase, Glycol chitosan, and COS, respectively, and i) representative photographs of dioxygen bubbling at 5 min reaction, respectively. j) ^{1}H NMR results of Glycol chitosan and Chitosan oligosaccharide (COS) to demonstrate catalase-like activity. After decomposing H_2O_2 (80×10^{-3} M) into a hydroxyl radical (•OH) through HRP (1000 unit mL^{-1}), Glycol chitosan and COS were added to confirm the formation of hydroxylamine by amine oxidation. Peaks around 6.5–7.2 ppm (blue arrow) indicate newly formed hydroxylamine after oxidation with •OH

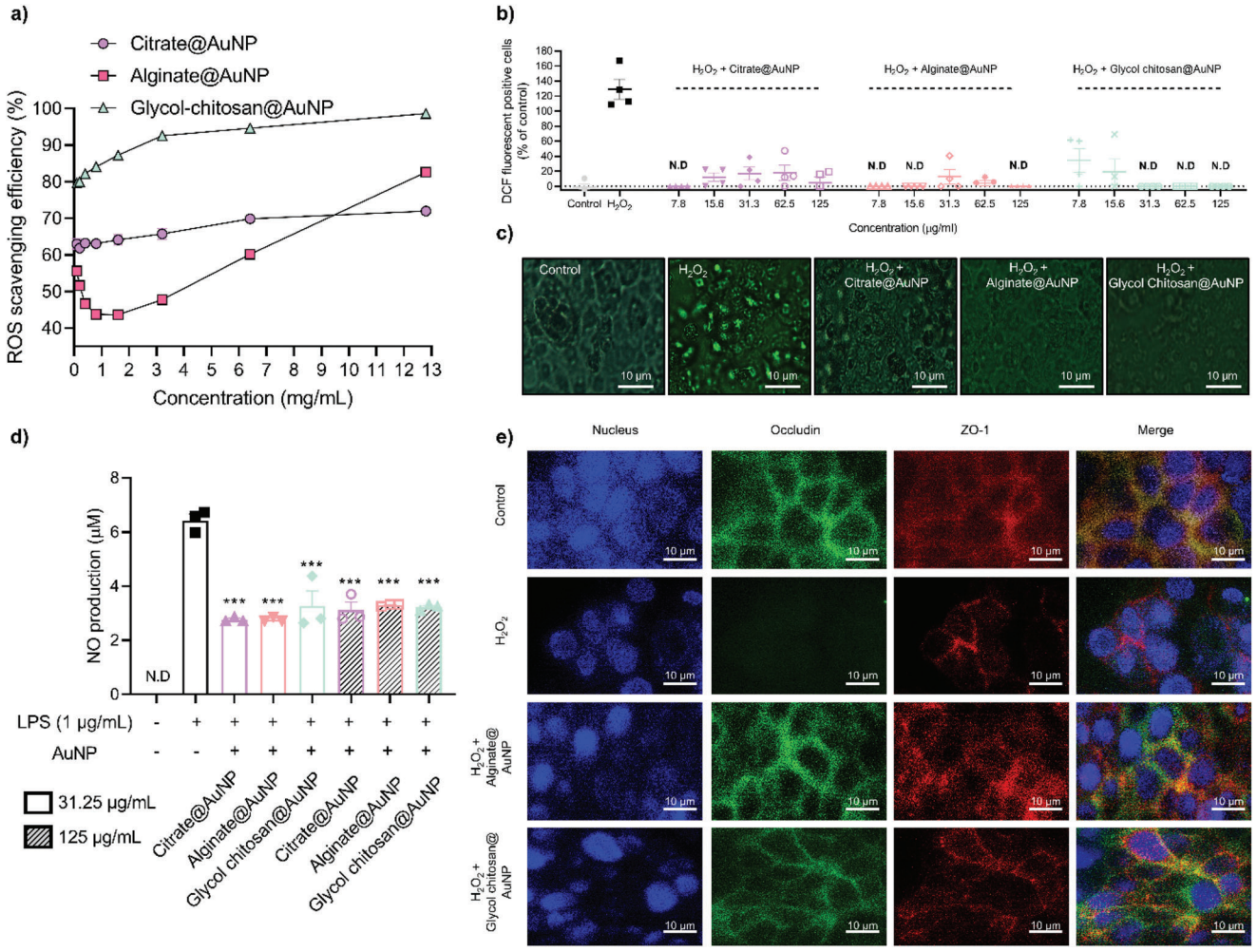

Figure 3. ROS/RNS scavenging efficacy of Citrate@AuNP, Alginate@AuNP, and Glycol chitosan@AuNP. a) ABTS assay for total ROS and scavenging assessment. b) DCF-DA assay of Caco-2 cells incubated with Citrate@AuNP, Alginate@AuNP, and Glycol chitosan@AuNP at a concentration from ≈7.8 to 125 μg mL^{-1}, respectively. N.D. stands for nondetectable. Data are expressed as mean ± SEM ($n = 4$). c) Fluorescence microscopic images of DCF-DA stained Caco-2 cells. Scale bar: 10 μm. d) Investigation of the RNS scavenging efficacy of Citrate@AuNP, Alginate@AuNP, and Glycol chitosan@AuNP at a concentration of 31.25 and 125 μg mL^{-1}, respectively, in LPS-induced NO_2^--producing RAW 264.7 cells. Data are expressed as mean ± SEM ($n = 4$). ***$p < 0.001$ versus only the LPS (1 μg mL^{-1})-treated group. e) Fluorescence images of Caco-2 cells that co-stained with Occludin (green), ZO-1 (red), and followed by DAPI-nucleus staining (blue). Scale bar: 10 μm.

together, Aurozyme treatment appears to promote colonic epithelial and homeostatic recovery by mediating M1 polarization and reduction of proinflammatory cytokines and restoring M2 polarization to basal levels. These results observed in our IBD microenvironment model further suggest that Aurozyme exerts a nearly nonstimulatory effect on RAW 264.7 macrophages.[33]

2.7. Amelioration of Colitis by Orally Administered Aurozyme

Colonic adhesion of orally administered Aurozyme was explored (**Figure 5**a). The mucoadhesive properties of glycol chitosan extended colonic retention for 24 h. Aurozyme was 3.4 times more effective at increasing retention and 2.7 times more effective at reducing clearance compared to Alginate@AuNP. Bio-TEM images repeatedly showed prolonged colonic adhesions of Aurozyme, while Alginate@AuNP was barely detectable after 24 h (Figure 5b; and Figure S16, Supporting information). These results can be attributed to the electrostatic attraction between glycol chitosan (positively charged) and mucin (negatively charged), which is further accompanied by contributions from hydrogen bonding and hydrophobic interactions.[34] Aurozyme, mainly observed in subepithelial goblet cells known to play a role in mucus secretion, consistently demonstrated mucoadhesive properties (Figure S17, Supporting Information). The delayed blood entry of the drug over 24 h was also due to mucoadhesion (Figure S18, Supporting Information). Based on several beneficial properties, including ROS/RNS-, HMGB1-scavenging effects, and prolongation of colonic mucus adhesion, next we sought to decipher the role of the scavenging effect of Aurozyme on multihazard signals in the DSS-induced colitis mice model.

Mice were given with 2.5% w/v DSS for 7 days and administered orally daily with Glycol chitosan@AuNP or Aurozyme until sacrifice (Figure 5c). Body weight changes were monitored to

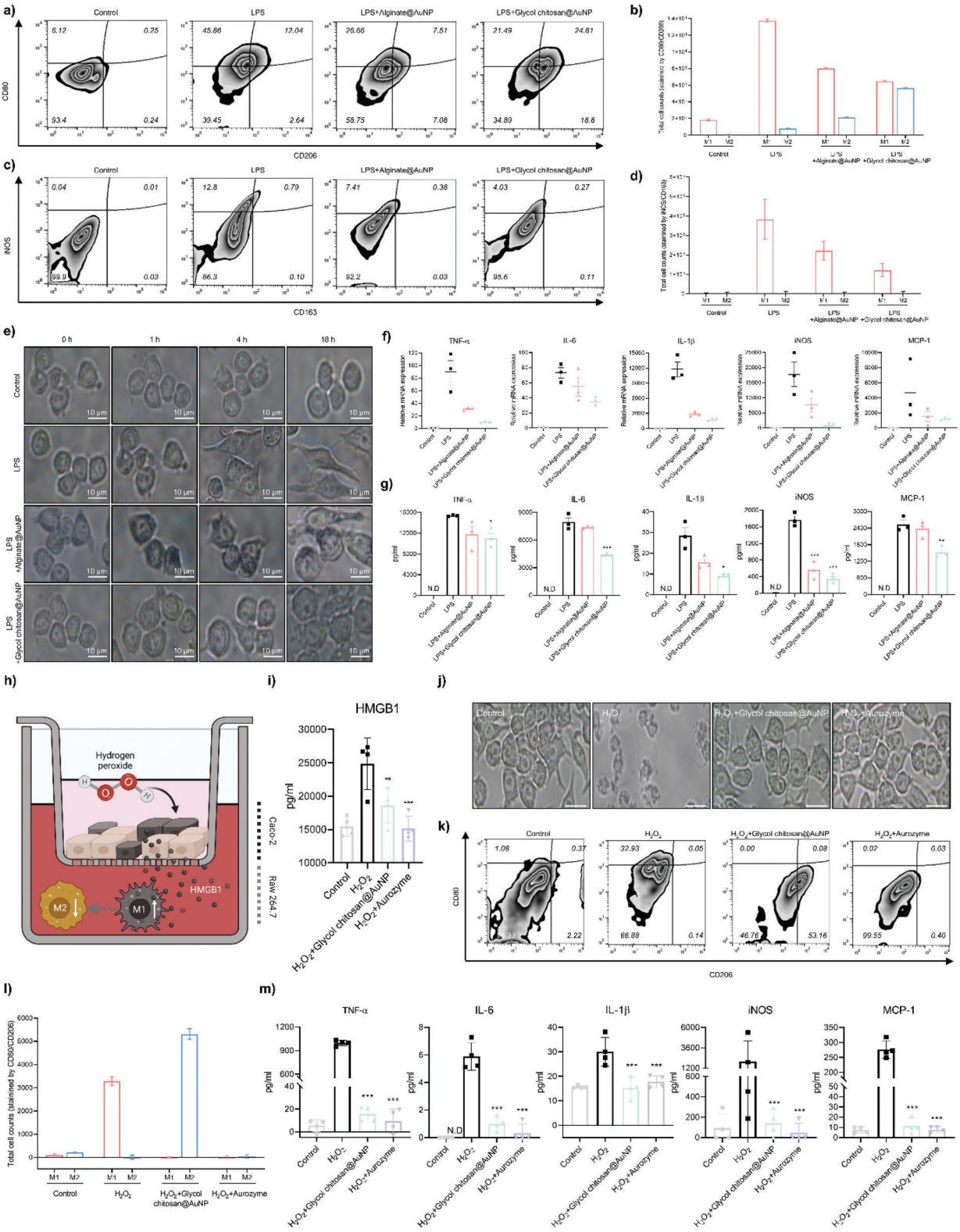

Figure 4. Multiple hazard signal scavenging of Aurozyme in the colitis-mimicking microenvironment. a–d) Effects of Citrate@AuNP, Alginate@AuNP, and Glycol chitosan@AuNP on M1 and M2 polarization in RAW 264.7 cells stimulated with LPS by measuring the expression of cell surface markers with flow cytometry. M1 cell surface markers included CD80 and iNOS; M2 cell surface markers included CD206 and CD163. Filled histograms represent iso-type-matched control antibody staining. Graph of total cell counts indicates mean fluorescence intensity of stained cells. Data are expressed as mean ± SEM ($n = 3$). e) Morphological investigation of RAW 264.7 cells stimulated with LPS. f) qRT-PCR results of proinflammatory cytokines (TNF-α, IL-6,

evaluate disease improvement (Figure 5d). PBS treatment (vehicle group) resulted in an ≈21.4% body weight loss at day 11 and mortality at days 5 and 12, respectively (Figure 5e). Inflammation such as diarrhea and rectal bleeding worsened during the treatment (Figure S19a,S19b, Supporting Information). Conversely, treatment groups (Glycol chitosan@AuNP or Aurozyme) had a 100% survival rate, recovered body weight loss from day 10, and the symptoms turned favorable toward the end of modeling with a lower DAI score (Figure 5f). These groups reversed DSS-induced colon shortening, alleviated edema, mitigated intestinal barrier disruption, recovered tight junction proteins, lowered the histological scores, and restored the mucus layer (Figure 5g,j; and Figures S19c–S19e, and S20, Supporting Information). Notably, Aurozyme treatment lowered HMGB1 levels even compared to healthy mice and stabilized ROS levels (Figure 5k,l). Ascribed to its stable attachment and multiscavenging effect of Aurozyme on colonic mucus, Aurozyme significantly reduced proinflammatory cytokines in both protein and mRNA levels and decreased the proportion of proinflammatory $CD80^+/CD45^+$ monocytes in the colonic leukocyte (Figure 5m; and Figure S21, Supporting Information).

2.8. Downregulation of Systemic Inflammation and Restoration of Gut Microbiota

Histopathological abnormalities, spleen enlargement, biochemical, and CBC tests were explored 14 days after oral administration of Glycol chitosan@AuNP and Aurozyme (Figures S22–S24, Supporting Information). No evidence of tissue inflammation or splenomegaly was observed, and vital organ functions remained within normal limits. DSS-challenged mice increased C-reactive protein (CRP) levels, which returned to normal with Aurozyme treatment (Figure S25a, Supporting Information). Calprotectin levels were investigated to characterize the colitis-induced inflammation. Levels of calprotectin, a DAMP (S100A8/9) species distinct from HMGB1, were reduced by Aurozyme treatment, indicating that the superb anti-inflammatory system achieved great relief in multifocal colitis (Figure S25b, Supporting Information).

Imbalances of the gut microbiota implicated in a variety of inflammatory and immune disorders play a critical role in the pathogenesis of IBD.[35,36] Therefore, concurrent restoration of the gut microbiota and immune homeostasis may complement each other in the successful treatment of colitis. To this end, fecal analysis by 16S ribosomal RNA gene sequencing was performed. As result, the DSS challenge significantly changed the composition of microflora compared to the control (healthy) group, whereas the Aurozyme treatment improved the richness and diversity of enterobacteria in the DSS-challenged mice (**Figure 6**a–c). The β-diversity between healthy mice and DSS-challenged mice treated with Aurozyme were mostly associated, indicating that restoration of gut immune homeostasis was achieved without perturbation of the gut microbiome (Figure 6d–g). Further analysis at the phylum and family level confirmed that Aurozyme treatment significantly increased the microflora associated with protective intestinal barrier function (*Akkermansia muciniphila*),[37] and beneficial roles in IBD (*Lactobacillus intestinalis*),[38] and obligatory anaerobe to alleviate DSS-induced colitis (*Muribaculum intestinale*)[39] (Figure 6e–j). In contrast, *Turicibacter sanguinis*, which is highly correlated with acute colitis, was found to be reduced.[40]

3. Discussion

The conventional intervention for the increasing incidence of IBD suffers from limited efficacy and systemic side effects due to a lack of control over its multifaceted etiology. Recent studies have explored several strategies for regulating danger signals in the pathogenesis of IBD. It has been proposed to deliver small molecule therapeutics by hydrogel to target inflamed extrudates.[41] Moreover, various nanomedicine has been introduced to modulate cell-free DNA (cfDNA) as a DAMP[42] and/or ROS/RNS.[43] Although these treatments have succeeded in remediating the severity of the disease, they are less patient-friendly due to limitations such as not inhibiting •OH, a detrimental factor in the biological system, or requiring repeated administration of stoichiometric antioxidants. By exploitation of the mucoadhesive properties of Glycol chitosan and enzyme-like properties of AuNP, here, we newly developed a mucoadhesive gold-based nanozyme (Aurozyme) with ROS/RNS scavenging only by SOD- and catalase-like activity. The glycol chitosan coating layer of AuNPs effectively scavenges •OH by decomposing H_2O_2 into water and oxygen molecules with high amine oxidation activity. Therefore, the intrinsic peroxidase-like activity of AuNP-based nanozyme could be successfully addressed into catalase-like activity beneficial for antioxidant therapy. Due to the lack of corresponding enzymes that scavenge •OH in living organisms,[44] nanozymes possess several advantages over enzyme-based therapeutics, including multiple enzyme-like activities, ease of fabrication, substantial stability, and minimal immunogenicity. In our study, the colloidal stability of Aurozyme was stable against acidic pH and exerted significant ROS/RNS scavenging activities. Moreover, the antioxidant therapeutic effect was remarkably extended by the prolongation of colonic residence time mediated by the ionic interaction between the cations of Glycol chitosan and the anions of the mucus layer.

In addition to ROS/RNS, DAMP such as HMGB1 also play a crucial role in intestinal epithelium damage and chronic colitis.[16,45] In colitis, HMGB1 is released by epithelium disruption and accelerates inflammation through binding to a re-

IL-1β, iNOS, and MCP-1). Data are expressed as mean ± SEM ($n = 3$). g) Investigation of pro-inflammatory cytokines (TNF-α, IL-6, IL-1β, iNOS, and MCP-1) by ELISA. Data are expressed as mean ± SEM ($n = 3$). h) Schematic illustration of colitis microenvironment in the trans-well culture system. i) Protein level of HMGB1 in the basolateral side of each group after treatment in the apical side of the trans-well system. Data are expressed as mean ± SEM ($n = 4$). $^{**}p < 0.01$ and $^{***}p < 0.001$ versus only H_2O_2-treated group. j) Representative morphological images of RAW 264.7 cell of each group in the trans-well system. k) Flow cytometry analysis of RAW 264.7 cell of each group in the trans-well system. l) Quantitative of total cell counts of M1/M2 macrophages stained by CD80/CD206 after the trans-well culture system ($n = 3$). m) The secreted amount of proinflammatory cytokines (TNF-α, IL-6, IL-1β, iNOS, and MCP-1) in the basolateral side of each group after the trans-well culture system. Data are expressed as mean ± SEM ($n = 4$). $^{***}p <$ 0.001 versus only H_2O_2-treated group.

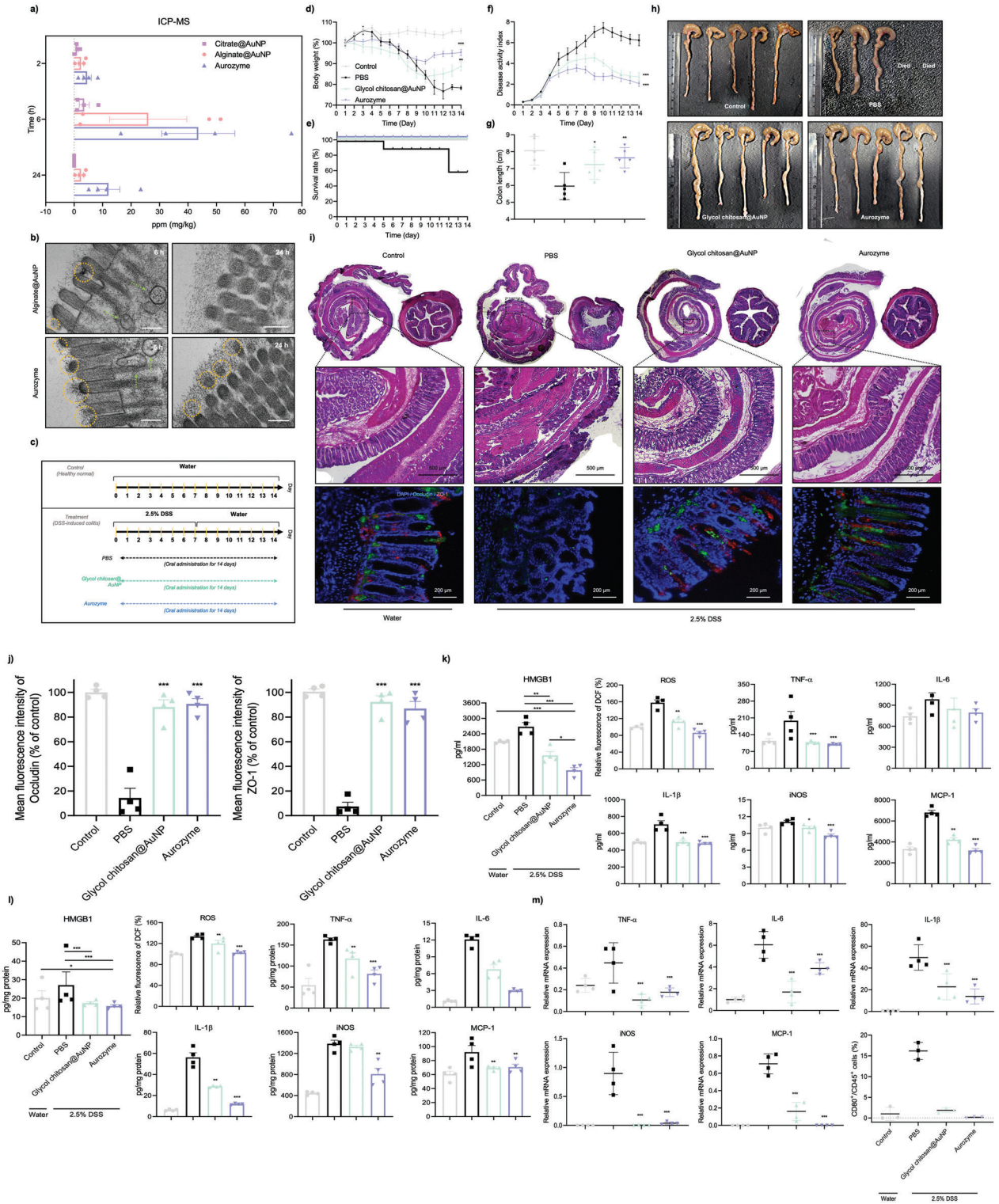

Figure 5. Evaluation of the efficacy of Aurozyme treatment in colitis. a) Quantification of colonic adhesion of Alginate@AuNP and Aurozyme by ICP-MS. Data are expressed as mean ± SEM ($n = 4$ biological independent animals). b) Bio-TEM images of colonic tissue at 6 and 24 h after oral administration of Alginate@AuNP and Aurozyme, respectively. Yellow circles indicate AuNPs entrapped in colonic mucus. Green arrows indicate goblet cells. Scale bar: 200 nm. c) Schematic illustration of the treatment plan. Mice were orally administered with PBS or 10 mg kg^{-1} of Glycol chitosan@AuNP and Aurozyme, respectively. d) Daily body weight changes in each group for 14 days. Data are expressed as mean ± SEM ($n = 5$ biological independent animals). $^{**}p <$

ceptor for advanced glycation end products (RAGE) and toll-like receptor (TLR) −2, −4, and −9 of immune cells.[46] Recently, HMGB1 is regarded as a boosting mediator in proinflammatory response by constituting highly immunostimulatory complexes with endotoxins, thereby potentiating proinflammatory cytokine secretion.[47] Intervention with HMGB1 antagonist is urged to address multietiological colitis, to this end, we investigated synergistic effects by modulating HMGB1 with Aurozyme, the nanozyme grafted with GL. Colitis-derived HMGB1 was attenuated by the GL-grafted Aurozyme, which in turn suppressed the subsequent inflammatory response. Collectively, the orally administered Aurozyme accumulated in damaged colonic epithelium for extended periods, and modulation on multihazard signals (ROS/RNS and HMGB1) were successfully achieved. Attributed to the multibeneficial properties of Aurozyme, the expression level of tight junction proteins was upregulated, while restoring intestinal barrier functions. Additionally, Aurozyme exerted a potent immune-modulatory effect in the region of lamina propria, characterized by a reduction in M1 polarization and proinflammatory cytokine expression. Representative indices of disease severity were recovered with the Aurozyme treatment. Meanwhile, systemic inflammation and side effects derived by repeated administration were negligible, thereby multitherapeutic efficacy and safety of Aurozyme play a decisive role in refractory chronic disease of colitis.[48]

It is increasingly recognized that the gut microbiome is pivotally responsible for intestinal homeostasis and overall health, and the dysregulated microbiome is implicated in numerous human diseases including IBDs.[49,50] Chitosan, serving as a probiotic, can alleviate some of the corresponding diseases by correcting imbalances in the gut microflora.[51] In particular, it is known to alleviate intestinal inflammation by up-regulating *Bifidobacteria* and *Lactobacilli* to improve intestinal villi and relative abundance (OTU richness) and diversity (Shannon diversity index) of the microflora.[52] Apart from other inorganic nanoparticles such as silver and zinc oxide (ZnO) that adversely affect the intestinal microflora, it recently reported that 4,6-diamino-2-pyrimidinethiol (DAPT) coated-AuNPs has a beneficial effect on intestinal microbial homeostasis (especially on *Akkermansia* and *Bifidobacterium*).[53] The basis on the above evidence, we investigated transitions in the gut microbiome after oral administration of Aurozyme. As results, it altered the gut microbiome, increasing the relative abundance and diversity of *Akkermansia muciniphila*, *Lactobacillus intestinalis*, and *Muribaculum intestinale*. It demonstrates the advantageous impact on gut microbiome: 1) *Akkermansia muciniphila*, which address the expression of tight junction and mucus production; 2) *Lactobacillus intestinalis*, known to improve intestinal villi and initiates anti-inflammation in colitis, and 3) *Muribaculum intestinale*, protective anaerobic bacteria against colitis.[54]

4. Conclusion

To our knowledge, this is the first biocompatible instance to switch peroxidase-like activities to catalase-like activities using AuNPs. The innovative converting technology of enzyme-like activity showcased by Aurozyme has opened up new avenues for exploring the complex interactions between nanomaterials and biological systems. Collectively, the remarkable properties of Aurozyme hold great promise for future advancements in nanomedicine.

5. Experimental Section

Materials: Gold(III) chloride trihydrate ($HAuCl_4$), peroxidase from horseradish (HRP, 279 IUs mg^{-1} solid), Catalase from bovine liver (2000–5000 IUs mg^{-1} protein), potassium persulfate, xanthine oxidase form bovine milk (0.4–1.0 IUs mg^{-1} protein), 5,5-Dimethyl-1-pyrroline *N*-oxide (DMPO), superoxide dismutase from bovine erythrocytes (SOD, 6045 IUs mg^{-1} protein), Griess reagent (modified), Glycyrrhizin (GL), sodium periodate(SP, NaIO4), 2-Mercaptoethanol, sodium cyanoborohydride solution($NaBH_3CN$), Ethylenediaminetetraacetic acid disodium salt dihydrate (EDTA) were purchased from Sigma-Aldrich (St. Louis, MO). the 2"-7"dichlorofluorescin diacetate (H_2DCFDA), Diethylenetriaminepentaacetic acid (DTPA), and trisodium citrate dihydrate were purchased from Thermofisher Scientific (Waltham, MA) and hydrogen peroxide 30% was purchased from Daejung (Gyeonggi, Korea). 4',6-diamidino-2-phenylindole (DAPI) was purchased from Vector Laboratories (Burlingame, CA). Sodium alginate with low viscosity and a G/M ratio (≥1.5) was purchased from Pronova UP LVG, FMC BioPolymer (Philadelphia, PA). Glycol chitosan was from FUJIFILM Wako chemicals (Osaka, Japan) and Hypoxanthine was purchased from TCI chemicals (Tokyo, Japan). Chitosan Oligosaccharide was purchased from TCI chemicals (Tokyo, Japan). The primer sequences used were as follows (**Table 1**)

Experimental Cell Lines and Animals: In vitro experiments were performed using the human epithelial colorectal cell line (Caco-2; Korean Cell Line Bank, Seoul, Korea) and macrophage cell line (Raw 264.7 cell; Korean Cell Line Bank, Seoul, Korea). Both cell lines were cultured using Dulbecco's Modified Eagle's Medium (DMEM, high glucose, Welgene, Gyeongsangbuk-do, Korea) containing 10% Fetal Bovine Serum (CELLectTM, Gold, 13 US Origin), 1% penicillin-streptomycin (Gibco, USA) in standard culture conditions at 37 °C and 5% CO_2. In vivo experiments were carried out using a 7-week-old male Balb/c mouse (Nara-Bio Company, Seoul, Korea) and C57/BL6 (OrientBIO, Seongnam, Korea) mouse. All animals were housed in specific pathogen-free conditions and maintained under the Institutional Animal Care and Use Committee (IACUC: 2022-0146) at Hanyang University.

0.01 and ***$p < 0.001$ versus PBS-treated 2.5% DSS-challenged mice. e) Survival rate of each group. Data are expressed as mean ± SEM ($n = 5$). f) DAI score of each group. Data are expressed as mean ± SEM ($n = 5$ biological independent animals). **$p < 0.01$ and ***$p < 0.001$ versus PBS-treated 2.5% DSS-challenged mice. g) Colon length in each group measured on day 14. Data are expressed as mean ± SEM ($n = 5$ biological independent animals). *$p < 0.05$ and **$p < 0.01$ versus PBS-treated 2.5% DSS-challenged mice. h) Images of the colon in each group on day 14. i) Representative images of the colon (Swiss roll and vertical section) from indicated groups were stained with H&E and immunofluorescence staining with anti-occludin (green), and anti-ZO-1 (red) antibodies. The nucleus was stained with DAPI. j) Mean fluorescence intensity for Occludin and ZO-1 using Image J software. Data are expressed as mean ± SEM ($n = 4$). ***$p < 0.001$ versus PBS-treated 2.5% DSS-challenged mice. k) HMGB1 and proinflammatory cytokines level in serum. Data are expressed as mean ± SEM ($n = 4$). *$p < 0.05$, **$p < 0.01$, and ***$p < 0.001$ versus PBS-treated 2.5% DSS-challenged mice. l) HMGB1 and proinflammatory cytokines level in colonic tissue. Data are expressed as mean ± SEM ($n = 4$). *$p < 0.05$, **$p < 0.01$, and ***$p < 0.001$ versus PBS-treated 2.5% DSS-challenged mice. m) mRNA level of proinflammatory cytokine in colonic tissue and population of M1-polarized macrophage ($CD80^+/CD45^+$). Data are expressed as mean ± SEM ($n = 4$). ***$p < 0.001$ versus PBS-treated 2.5% DSS-challenged mice.

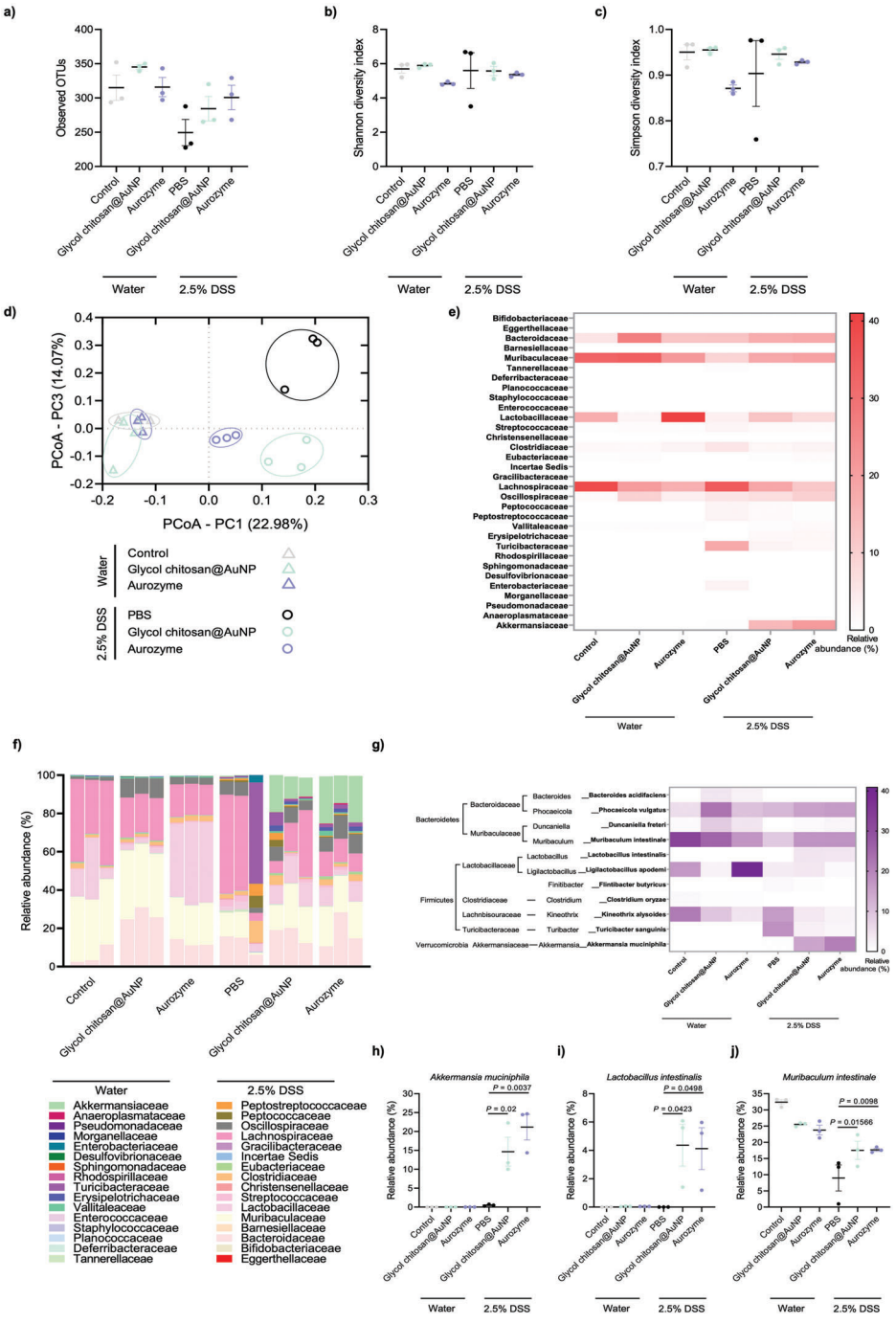

Figure 6. Aurozyme rehabilitates DSS-induced dysbiosis without microbiota perturbation. C57BL/6 mice were provided with 2.5% DSS in drinking water for 7 days. Mice were treated as above in Figure 5c. Feces collected on day 14 were analyzed for gut microbiome by 16S rRNA sequencing. a) Estimation of observed OTU richness. b) Shannon and, c) Simpson indices for α-diversity of the microbial community. d) Coordinates analysis for the gut microbiome β-diversity. The significance of clustering was determined using an analysis of similarities (ANOSIM). e) Heatmap of the relative abundance of microbial compositional profiling at a family-level taxonomy. f) Relative abundance of the gut microbiome. g) Heatmap of the relative abundance of phylum-species-level taxonomy. h) Relative abundance of *Akkermansia muciniphila* in microflora. i) Relative abundance of *Lactobacillus intestinalis* in microflora. j) Relative abundance of *Muribaculum intestinale* in microflora. Data are expressed as mean ± SEM ($n = 3$ biological independent animals). Statistical analysis was evaluated by Student's *t*-tests or one-way analysis of variance (ANOVA).

Table 1. The primer sequences used for detecting the inflammatory biomarkers.

GAPDH	Forward	CAGGAGGCATTGCTGATGAT
	Reverse	GAAGGCTGGGGCTCATTT
TNFα	Forward	CCCTCACACTCAGATCATCTTCT
	Reverse	GCTACGACGTGGGCTACAG
IL-6	Forward	TAGTCCTTCCTACCCCAATTTCC
	Reverse	TTGGTCCTTAGCCACTCCTTC
IL-1β	Forward	GCAACTGTTCCTGAACTCAACT
	Reverse	ATCTTTTGGGGTCCGTCAACT
MCP-1	Forward	TTAAAAACCTGGATCGGAACC
	Reverse	GCATTAGCTTCAGATTTACGGGT
iNOS	Forward	CCCCGCTACTACTCCATCAG
	Reverse	CCACTGACACTTCGCACAAA

Synthesis of Citrate@AuNP, Alginate@AuNP, and Glycol chitosan@AuNP: To synthesize Citrate@AuNP, citrate (final concentration: 5.69, 7.98, 11.3 mM) and gold(III) chloride trihydrate (1.13 mM) were dissolved in distilled water, respectively, and the gold solution was slowly dropped into citrate solution. The mixture was heated to 90 °C, while simultaneously stirring using a magnetic bar at 1000 rpm for 20 min. After cooling the solution, it was centrifuged at 43 700 g for 30 min (denoted the compounds as Citrate@AuNP (1:5), Citrate@AuNP (1:7), and Citrate@AuNP (1:10) in order of citrate concentration). For the synthesis of Alginate@AuNP, Alginate (0.2% and 0.4%, w/v) was dissolved in distilled water and heated to 90 °C. The gold solution (0.8 mM) was added dropwise to the Alginate solution. The remaining process was carried out the same as Citrate@AuNP (denoted the compounds as Alginate@AuNP 0.2% and Alginate@AuNP 0.4% in order of alginate concentration. For the synthesis of Glycol chitosan@AuNP, glycol chitosan (0.32% w/v) was dissolved in distilled water and heated to 90 °C. The gold solution (1.0 mM) was added dropwise to the Glycol chitosan solution. The remaining process was carried out in the same as Citrate@AuNP.

Characterization of Citrate@AuNP, Alginate@AuNP, Glycol chitosan@AuNP, and Aurozyme: The UV–visible spectrophotometer (NanoDrop 2000; Thermo Scientific, Wilmington, NC) was used to confirm the synthesis of AuNPs which has absorbance in 520–530 nm wavelength. The X-ray diffractometer (XRD, D8 ADVANCE, BRUKER, Germany) was used to confirm the presence of an Au atom. The TEM (Transmission Electron Microscope, JEM 2100F, JEOL, NC) was used to measure the size and lattice of AuNP using a Cu-TEM grid. Zetasizer (Nano ZS, Malvern Panalytical, Worcestershire, UK) was used to measure the charge, the poly diversity index (PDI), and dynamic light scattering (DLS) of AuNP. After making the solution to the pH of the biomimetic environment (pH 2 and 6), the colloidal stability was measured by UV–vis after 0, 1, 3, 6, 9, and 12 h. Also, the charge and DLS of AuNP were measured by Zetasizer after 12 h.

Confirmation of Superoxide Dismutase (SOD)-Like Properties of AuNP: ESR (Electron Spin Resonance spectrometer, EMXplus-9.5/12/P/L System, Bruker, Germany) assay was conducted to confirm the SOD-like activity of AuNP. DTPA (25 μM), hypoxanthine (1 mM), hypoxanthine oxidase (1 IU mL^{-1}), DMPO (1 M), and SOD (1000 IU mL^{-1}) were constituted in 100 mM phosphate buffer (pH 7.4). The DTPA (700 μL), DMPO (200 μL), and hypoxanthine (1 mL) were reconstituted to make final concentrations 17.5 μM, 10 mM, and 0.5 mM, respectively, and this mixture remained as an undiluted condition prior to making superoxide radical. After transferring 47.5 μL from the mixture solution, 2.5 μL of xanthine oxidase (0.05 IU mL^{-1}) was reacted for 30 s to serve as a positive control. The SOD solution was added to the mixture solution and reacted for 30 s to make a negative control. The Citrate@AuNP (1:10), Alginate@AuNP 0.2%, and Glycol chitosan@AuNP 0.32% were added to the positive control solution to make the final concentration of 125 μg mL^{-1}, respectively. The mixture was reacted for 2 min before measuring the ESR intensity.

Examination of Peroxidase and Catalase Properties of AuNP: To confirm the peroxidase-like activity of AuNP, AuNP (125 μg mL^{-1}) was added to the reaction solution of TMB and H_2O_2 (80×10^{-3} M, adjusted to pH 7.4, 5.8, and 2.1, respectively) and reacted for 5 min. HRP (1000 IU mL^{-1}) was reacted with reaction solution (TMB and H_2O_2) for 5 min to serve as a positive control. The color change was determined by the measurement of absorbance at 450 nm. Results of peroxidase-like activity (%) were normalized based on HRP activity at pH 5.8. Next, to test H_2O_2 consumption by the catalase-like activity of AuNP, H_2O_2 (80×10^{-3} M, adjusted to pH 7.4, 5.8, and 2.1, respectively), TMB, and AuNP (125 μg mL^{-1}) were reacted for 5 min. After, HRP solution (1000 IU mL^{-1}) was further added to detect the remaining H_2O_2. The color change was determined by the measurement of absorbance at 450 nm. Catalase-like activity is normalized based on Glycol chitosan@AuNP activity at pH 5.8.

^{1}H-NMR for Estimating the Catalase-Like Activity of Glycol Chitosan and COS (Chitosan Oligosaccharide): The amine oxidation of Glycol chitosan and COS were conducted through the reaction of the hydroxyl radical, and the resulting change in the functional group is confirmed by ^{1}H-NMR. Glycol chitosan (125 μg mL^{-1}) and COS (125 μg mL^{-1}) dissolved in D_2O (deuterium) were reacted with a mixture of HRP (1000 IU mL^{-1}) and H_2O_2 (80×10^{-3} M) for 5 min, respectively. The mixture was measured by ^{1}H-NMR (Nuclear Magnetic Resonance, VNMRS 600 MHz, Agilent Technologies).

Cytotoxicity Evaluation of AuNPs: The cell viability was determined by LDH Cytotoxicity Assay Kit (Abcam, Wuhan, Chin) Caco-2 cells (1×10^4 cells $well^{-1}$) were seeded on a 96-well plate and cultured in complete media for 48 h. Cells were washed with PBS and treated with Citrate@AuNP-, Alginate@AuNP-, and Glycol chitosan@AuNP-dissolved medium at a concentration of 7.8–125 μg mL^{-1}, respectively, for 36 h. 1% Triton X-100 (200 μL) was added to normal cells to serve as a positive control. Thereafter, each treatment medium (100 μL) was transferred to a tube containing LDH reaction solution (100 μL) and reacted for 30 min at 37 °C. After centrifuging the tube at 20 000 g for 15 min, the supernatant of the mixture was transferred to a microplate and measured absorbance at 565 nm. The cytotoxicity (%) was calculated as (A sample-A background)/(A maximum-A spontaneous) × 100. Raw 264.7 cells (1×10^4 cells $well^{-1}$) were seeded on a 96-well plate and cultured in complete media for 24 h. Cells were washed with PBS and treated with Citrate@AuNP-, Alginate@AuNP-, and Glycol chitosan@AuNP-dissolved medium at a concentration of 7.8 to 125 μg mL^{-1}, respectively, for 18 h. The remaining process was the same as the experimental method of the Caco-2 cell.

ABTS (2,2′-azinobis-(3-ethylbenzothiazoline-6-sulfonic acid) Assay: The ABTS assay was conducted to confirm the ROS radical scavenging ability of AuNP. To constitute ABTS radical (ABTS•) solution, an equal volume of ABTS (14 mM) and potassium persulfate (4.9 mM) was dissolved in deionized water. Then incubated the mixture overnight (12–16 h) at RT in the dark and measured the absorbance at 734 nm wavelength until 0.8 value was obtained. ABTS solution was added to the tube containing 500 μL of AuNP and incubated for 15 min with an orbital shaker (50 rpm). After centrifugation at 20 000 g for 10 min, the supernatant (100 μL) was transferred to a 96-well plate. Radical scavenging activity was determined by the absorbance at 734 nm and was calculated as I% = [(Abs0-Abs1) / Abs0] × 100 (Abs 0 indicates the absorbance of ABTS and ABS 1 indicates the absorbance of Sample).

RNS Scavenging Activity: NO (Nitric Oxide) Production: The concentration of NO was confirmed by the Griess reagent. Raw 264.7 cells were seeded in a 48-well plate (5×10^5 cells $well^{-1}$) for 24 h and then incubate cells in media with or without AuNPs (Citrate@AuNP, Alginate@AuNP, and Glycol chitosan@AuNP, respectively) for 5 h. After washing with PBS, cells were incubated for 20 h in media with or without LPS (1 μg mL^{-1}) dissolved in DMEM. The cell supernatants (100 μL) were transferred to a 96-well plate and mixed with an equal volume of Griess reagent for 10 min. Absorbance at 546 nm wavelength was measured. The concentration of NO was calculated by nitrite standard curve (0–10 μM).

Intracellular ROS Scavenging Activity: ROS scavenging activity in Caco-2 cells was evaluated by DCFH-DA. Caco-2 cells (1.0×10^4 cells $well^{-1}$)

were seeded in a 96-well plate and cultured for 48 h. Citrate@AuNP, Alginate@AuNP, and Glycol chitosan@AuNP (concentration of 7.8–125 μg mL^{-1}) were treated with a culture medium containing H_2O_2 (100 μM) for 4 h. Thereafter, cells were stained by DCFH-DA (final concentration 2 μM) for 15 min and washed with PBS. Intracellular ROS level was confirmed by the fluorescence measurement (excitation/emission: 490/520 nm).

Recovery of the Tight Junction: Caco-2 cells (1×10^6 cells $well^{-1}$) were seeded on a 6-well plate and incubated for 48 h. To confirm the recovery of tight junctions, cells were treated with Alginate@AuNP (125 μg mL^{-1}) and Glycol chitosan@AuNP (125 μg mL^{-1}) simultaneously with H_2O_2 (100 μM) for 4 h. Afterward, cells were washed with PBS and fixed in 4% paraformaldehyde for 10 min. The cells were repeatedly washed twice with PBS-Tween20 (PBS-T) for 2 min and incubated with 20% goat serum (PBS-T as a solvent) for 30 min at RT. Anti-ZO-1 (anti-rabbit ZO-1, ab59720, Abcam) and anti-Occludin (anti-mouse occludin, OC-3F10, Invitrogen) antibodies (1:100) were treated for 1 h at RT. After washing twice, cells were treated with secondary antibodies (goat anti-mouse-488 and goat anti-rabbit-594, 1:200) for 1 h at RT followed by DAPI mounting.

Observation of the M1 and M2 Polarization of Raw 264.7 Cells: To observe the ratio of M1 and M2 polarization when AuNP-treated Raw 264.7 cells were stimulated with LPS and measured by flow cytometry (BD FACS Calibur, BD bioscience, NJ). Raw 264.7 cells were seeded in a 100 mm dish (2.0×10^6 cells) and incubated for 24 h. The cells were washed with PBS and incubated for 5 h with or without AuNP (125 μg mL^{-1}). After collecting the cells with a scraper, centrifuge at 1200 rpm for 3 min and remove the supernatant. The cells were stained with antibodies according to the instruction on the product sheet. CD206 APC-eFluor 780 (MMR Monoclonal Antibody, eBioscience), CD80-FITC (B7-1 Monoclonal Antibody, eBioscience), CD 163-eFluor 450 (eBioscience), and iNOS-PE (eBioscience) were used. Cells were analyzed via flow cytometer ((BD FACS Calibur, BD bioscience, NJ).

Analysis of Proinflammatory Cytokines: qRT-PCR (Quantitative reverse transcription polymerase chain reaction) and ELISA (enzyme-linked immunosorbent assay) analysis were conducted to evaluate the secretion of proinflammatory cytokines in LPS-stimulated Raw 264.7 cells. Raw 264.7 cells were seeded in a 12-well plate (1.0×10^5 per well) and cultured in complete media for 24 h. AuNPs (Alginate@AuNP 125 μg mL^{-1}, Glycol chitosan@AuNP 125 μg mL^{-1}) were incubated for 5 h. The cells were further treated with LPS (1 μg mL^{-1}) for 20 h. RNA extraction was performed using QIAzol Lysis Reagent and RNeasy Mini Kit (QIAGEN, Germany) and reverse transcribed into cDNA by iscript cDNA synthesis kit (BIO RAD Laboratories, USA). After preparing equal amounts of cDNA from the extracted RNA, the relative gene expression levels were quantified by RT-PCR (Applied Biosystems 7500, USA). Each sample was compared to the GAPDH control and calculated using the ΔΔCt method. The protein level of TNF-α, IL-6, IL-1 β, MCP-1, and iNOS were determined by ELISA kit. TNF-α (EliKine Mouse TNF-α ELISA Kit, Abbkine), IL-6 (IL-6 Mouse ELISA Kit, Invitrogen) IL-1 β (IL-1 beta Mouse ELISA Kit, Invitrogen), MCP-1 (MCP-1 Mouse ELISA Kit, Invitrogen), iNOS (Mouse NOS2/iNOS ELISA Kit, Elabsciecne).

Conjugation of Glycol Chitosan-Glycyrrhizin (Glycol Chitosan-GL): Glycyrrhizin (GL, 1 mM) was dissolved in DW, and adjusted pH using 1 N sodium hydroxide until it was completely dissolved in the solution. Next, sodium periodate (SP, 1 mM) was separately added to DW and kept in the dark. The GL solution was added dropwise into the SP solution to form oxidized GL (oGL). Stirred the GL solution for 30 min in the dark and in a light state for 30 min. Glycol chitosan (0.32% w/v) was dissolved in DW in an equal volume as the oGL solution. Then use 1.0 M HCl to adjust the pH until Glycol chitosan is completely dissolved in the solution. Dropwise the oGL solution into the Glycol chitosan solution. The solution was reacted for 2 h at 4 °C. Sodium cyanoborohydride was added in an amount equivalent to 1/1000 of the total solution. The solution was reacted overnight at 4 °C and dialyzed with a dialysis cellulose bag (MWCO 3.5 kDa, VISKASE, IL).

Synthesis of Aurozyme: Glycol chitosan-GL conjugate (0.32% w/v) was added to distilled water, pH adjusted using 1 N NaOH until dissolved, and heated to 90 °C on a hot plate. AuNP solution (1 mM) was added dropwise into the Glycol chitosan-GL solution and stirred for 30 min. The solution was centrifuged (43 700 g, 30 min) and the pellet was reconstituted in DW.

Trans-Well Culture: Caco-2 cells (2.5×10^4 cells $well^{-1}$) were seeded in the apical side of Transwell insert with a 6.5 mm diameter and 0.4 μm pore size, and Raw 264.7 cells (5.0×10^4 cells $well^{-1}$) were seeded in each well of the culture plate. After insertion of the transwell into each well of the plate, Glycol chitosan@AuNP and Aurozyme (125 μg mL^{-1}) along with H_2O_2 (100 μM) were treated in the apical side of the transwell and were incubated for 24 h. Following this, the levels of HMGB1, TNF-α, IL6, IL-1β, MCP-1, and iNOS in the basolateral side of the transwell were measured using ELISA.

Quantification of Mucoadhesive AuNPs (Alginate@AuNP and Aurozyme): Balb/c mice were orally administered by Alginate@AuNP and Aurozyme, respectively. After 2, 6, and 24 h, mice were sacrificed and the colons without feces were fixed with 4% paraformaldehyde and the samples were prepared for Inductively Coupled Plasma-Mass Spectrometry (ICP-MS, iCAP RQ, Thermo Fisher Scientific) analysis. The exact weights of the dissected colon were measured in a borosilicate glass tube and nitric acid (800 μL, 70%) was added. The sample glass tubes were heated at 60 °C water bath for 3 h. Thereafter, HCl (37%) was further added to digest colon tissue and adjusted to nitric acid (2%) and HCl (0.5%) with DW. The solutions were filtered using pore-size filters (0.22 μm) and analyzed by the ICP-MS. The Au concentration in the sample was quantified by using a standard curve of Au (0.0001–0.05 μg mL^{-1})

Bio-TEM of Colonic Tissue: Balb/c mice were orally administered by Alginate@AuNP and Aurozyme, respectively. After 6, and 24 h, mice were sacrificed and the colons without feces were fixed with 4% paraformaldehyde and the samples were prepared for Bio-TEM (Talos L120C, FEI, Czech). Sorensen's phosphate buffer, which is composed of solutions A and B (A is 0.2 M $Na_2HPO_4 \cdot 2H_2O$ and B is 0.2 M $NaH_2PO_4 \cdot H_2O$), was added for 10 min to rinse off the fixative. Next, 1% osmium tetroxide (OsO_4) was added for 1 h and repeatedly washed with Sorensen's phosphate buffer for 10 min to eliminate the remaining OsO_4. Dehydration of the samples was performed with different concentrations of ethanol as follows: 30% (10 min); 50% (10 min); 70% (10 min); 90% (10 min); and finally, 100% (20 min, 3 times). The formation of epoxy resin block with a low-viscosity embedded media Spurr's Kit method was applied to all the samples. The epoxy resin specimens were cut into 80 nm thick sections using an ultramicrotome (EM UC7, Germany), and the obtained sections were air-dried for at least 1 h. Copper grids were mounted with 2% uranyl acetate for 20 min, briefly washed with distilled water, and mounted onto lead citrate (0.4%) for staining for 10 min. The section placed on the grid was observed using an 80 kV TEM.

DSS-Induced Model of IBD: 7-week-old male C57BL/6 mice were housed in groups of five mice per cage and acclimatized for 1 week before inclusion in the study. Mice received 2.5% w/v DSS supplemented in drinking water (sterilized) for 7 days, followed by normal water. Control mice were provided with normal water only. Then PBS, Glycol chitosan@AuNP (10 mg kg^{-1}), and Aurozyme (10 mg kg^{-1}) were administered via an oral into mice for 14 consecutive days. Body weight was measured daily for 14 day experimental period. The DAI was scored using the following criteria: stool consistency (hard: 0, soft: 2, and diarrhea: 4), fecal occult blood (negative: 0, positive: 2, and macroscopic: 4), and weight loss (less than 1%: 0, 1 to 5%: 1, 5 to 10%: 2, 10 to 20%: 3, and more than 20%: 4). On the last day of the experiment, mice were sacrificed, and the entire colon and organs were excised and measured the colon length of each group. Then, three distal slices 1 and 0.5 cm long, respectively, were used to evaluate cytokines and macrophage polarization.

Ex Vivo Analysis of HMGB1 and Proinflammatory Cytokines: At the end of the study, blood samples were obtained via cardiac puncture, and colonic tissues were surgically harvested. The tissues were first dissected and immediately frozen in liquid nitrogen. To extract the protein, 300 μL of chilled RIPA lysis buffer (Sigma-Aldrich, Saint Louis, MO) per 5 mg of tissue, followed by homogenization using a FastPrep-24TM 5G bead beating system (MP Biomedicals, LLC, USA), was added. The resulting supernatant was collected by centrifugation at 20 497 g for 3 min at 4 °C. HMGB1, TNFα, IL-6, IL-1β, MCP-1, and iNOS concentration in plasma and colonic tissues were determined enzymatically with ELISA, the

supernatant was collected. The amount of HMGB1 and proinflammatory cytokines in colon homogenates were quantified by ELISA kit.

Ex Vivo Analysis of mRNA: Samples of the end section of the colon were immersed in liquid nitrogen and frozen. The 600 µL of RLT buffer (RNeasy Mini Kit, QIAGEN) per 30 mg of tissue was added and 10 µL of 2-mercaptoethanol (Sigma) was added per 1 mL of RLT buffer. After homogenizing through a homogenizer (FastPrep-24TM 5G bead beating system, MP Biomedicals, LLC, USA), the supernatant was collected by centrifugation at 20 497 g for 3 min at 4 °C. After adding an equal volume of 70% EtOH to the supernatant, pipetting immediately. And then mRNA was extracted from tissues using the RNeasy Mini Kit. 1.0 µg of total RNA was reverse transcribed to cDNA using an iscript cDNA synthesis kit. After preparing equal amounts of cDNA from the extracted RNA, the relative gene expression levels were quantified by RT-PCR (Applied Biosystems 7500, USA). Each sample was compared to the GAPDH control and calculated using the ΔΔCt method. The primer sequence is the same as the sequence used in vitro experiment.

Ex Vivo Macrophage Population Analysis: Colon tissues were harvested and then Payer's patch and fat were removed. The tissue was cut lengthwise and washed 3 times with cold PBS. The dissected colon tissue was cut horizontally by 1 cm and placed in RPMI (FBS 10%, PS 1%) containing EDTA (2 mM). To separate the cells of the epithelial cell layer, the samples were placed in an incubator (37.5 °C, 250 rpm, 40 min). Then, the solution was filtered using a 70 µm cell strainer and centrifuged at 1500 rpm, 4 °C for 10 min. The total colonic cells were stained with anti-CD45- APC-Cy7 (BD harmingen, San Diego, USA) anti-CD80-FITC and anti-CD206 APC-eFluor 780 to classify the lymphocyte population and stain M1 and M2, respectively. The relative mean fluorescence intensity for each macrophage was analyzed by using flow cytometry.

Histological Analysis and Immunofluorescence Staining of Tissue: Tissues were fixed in 4% paraformaldehyde and tissue processing was performed automatically with the Leica TP1020 semienclosed Benchtop Tissue Processor (Leica Biosystems, Wetzlar, Hesse, Germany). After embedding in paraffin, paraffin blocks were sliced at 7 µm thickness using a Leica RM 2145 Microtome (Leica Biosystems). For histological analysis, hematoxylin and eosin-stained colon tissue sections were prepared. For immunofluorescence staining, the paraffin sections were blocked with 5% of bovine serum albumin blocking solution for 1 h and incubated with antioccludin, anti-ZO-1, and anti-MUC-2 antibodies at RT. After washing twice, cells were treated with secondary antibodies (goat anti-mouse-488 and goat anti-rabbit-594, 1:200) for 1 h at RT followed by DAPI mounting.

Biochemical and Hematological Tests: Normal BALB/c mice were orally administered with PBS, Glycol chitosan@AuNP (10 mg kg^{-1}), and Aurozyme (10 mg kg^{-1}) for 14 consecutive days. The blood was collected by cardiac puncture and obtained serum (100 µL, for the biochemistry test) and plasma (200 µL, for the CBC test). Samples were referred to Daegun Health Care Co. (DK Korea, Seoul, South Korea) for CBC ($n = 4$) and biochemical tests ($n = 4$).

5.0.0.1. rRNA Microbiota Sequencing, Taxonomic Classification, and Diversity Studies: Fecal samples were taken from mice on day 14 and stored at −80 °C, and samples were referred to Macrogen (Seoul, South Korea). Briefly, sequencing libraries of the V3 and V4 regions were constructed using the MiSeq Illumina sequencing platform. The 16S rRNA amplicons were amplified using V3–V4 region primers. Sequences were assigned to OTUs using a cutoff value of 0.03 and classified against the Ribosomal Database Project 16S rRNA gene training set (v.9) with an 80% confidence threshold for taxonomic classification. Alpha diversity was measured by the Chao1 and Shannon indices, and the generalized UniFrac (GUniFrac) method was applied for phylogenetic distance calculations. Unweighted UniFrac measurements for beta diversity were plotted along two principal coordinates based on 10 000 readings per sample. ANOSIM analyses were performed with the vegan package (v2.5-7) in R (v4.0.5) to compare the similarities among different groups. Data visualization was performed in GraphPad Prism (version 8.3.0; GraphPad Software Inc., San Diego, CA).

Statistics: All data were presented as mean ± S.E.M (standard error of the mean). Statistical analysis was evaluated by Student's *t*-tests or one-way analysis of variance (ANOVA). *p*-value less than 0.05 was considered a statistically significant value. GraphPad Prism (version 8.3.0; GraphPad Software Inc., San Diego, CA) was used for statistical analyses.

Supporting Information

Supporting Information is available from the Wiley Online Library or from the author.

Acknowledgements

This research was supported by the National Research Foundation of Korea (NRF) grant funded by the Korea government (MSIT) (Nos. NRF-2022R1A4A1030421 and NRF-2020R1A2C3005834)

Conflict of Interest

The authors declare no competing financial interest.

Author Contributions

H.S.K. and S.L. contributed equally to this work. H.S.K., S.L., and D.Y.L. conceived the research design, performed the experiments, conducted data processing, contributed to the analysis and interpretation of data, and grafted the manuscript. H.S.K. and D.Y.L. edited the manuscript.

Data Availability Statement

The data that support the findings of this study are available from the corresponding author upon reasonable request.

Keywords

catalase-like activity, glycol chitosan, gold nanoparticles, inflammatory bowel diseases, nanozymes, reactive nitrogen species (RNS), reactive oxygen species (ROS)

Received: March 19, 2023
Revised: May 15, 2023
Published online:

[1] S. Alatab, S. G. Sepanlou, K. Ikuta, H. Vahedi, C. Bisignano, S. Safiri, A. Sadeghi, M. R. Nixon, A. Abdoli, H. Abolhassani, V. Alipour, M. A. H. Almadi, A. Almasi-Hashiani, A. Anushiravani, J. Arabloo, S. Atique, A. Awasthi, A. Badawi, A. A. A. Baig, N. Bhala, A. Bijani, A. Biondi, A. M. Borzì, K. E. Burke, F. Carvalho, A. Daryani, M. Dubey, A. Eftekhari, E. Fernandes, J. C. Fernandes, et al., *Lancet Gastroenterol. Hepatol.* **2020**, *5*, 17.

[2] J. Halfvarson, C. J. Brislawn, R. Lamendella, Y. Vázquez-Baeza, W. A. Walters, L. M. Bramer, M. D'amato, F. Bonfiglio, D. Mcdonald, A. Gonzalez, E. E. Mcclure, M. F. Dunklebarger, R. Knight, J. K. Jansson, *Nat. Microbiol.* **2017**, *2*, 17004.

[3] K. M. Taylor, P. M. Irving, *Nat. Rev. Gastroenterol. Hepatol.* **2011**, *8*, 646.

[4] C. N. Bernstein, M. Fried, J. H. Krabshuis, H. Cohen, R. Eliakim, S. Fedail, R. Gearry, K. L. Goh, S. Hamid, A. G. Khan, A. W. Lemair, Malfertheiner, Q. Ouyang, J. F. Rey, A. Sood, F. Steinwurz, O. O. Thomsen, A. Thomson, G. Watermeyer, *Inflamm. Bowel Dis.* **2010**, *16*, 112.

[5] S. Zhang, Y. Li, S. Sun, L. Liu, X. Mu, S. Liu, M. Jiao, X. Chen, K. Chen, H. Ma, T. Li, X. Liu, H. Wang, J. Zhang, J. Yang, X.-D. Zhang, *Nat. Commun.* **2022**, *13*, 4744.
[6] H. Wei, E. Wang, *Chem. Soc. Rev.* **2013**, *42*, 6060.
[7] Y. Song, K. Qu, C. Zhao, J. Ren, X. Qu, *Adv. Mater.* **2010**, *22*, 2206.
[8] Y. Huang, J. Ren, X. Qu, *Chem. Rev.* **2019**, *119*, 4357.
[9] Y. Liu, Y. Cheng, H. Zhang, M. Zhou, Y. Yu, S. Lin, B. Jiang, X. Zhao, L. Miao, C.-W. Wei, Q. Liu, Y.-W. Lin, Y. Du, C. J. Butch, H. Wei, *Sci. Adv.* **2020**, *6*, eabb2695.
[10] J. Lou-Franco, B. Das, C. Elliott, C. Cao, *Nano-Micro Lett.* **2021**, *13*, 10.
[11] B. Jiang, M. Liang, *Chin. J. Chem.* **2021**, *39*, 174.
[12] L. Gao, J. Zhuang, L. Nie, J. Zhang, Y. Zhang, N. Gu, T. Wang, J. Feng, D. Yang, S. Perrett, X. Yan, *Nat. Nanotechnol.* **2007**, *2*, 577.
[13] H. Dong, W. Du, J. Dong, R. Che, F. Kong, W. Cheng, M. Ma, N. Gu, Y. Zhang, *Nat. Commun.* **2022**, *13*, 5365.
[14] J. Chen, Q. Ma, M. Li, D. Chao, L. Huang, W. Wu, Y. Fang, S. Dong, *Nat. Commun.* **2021**, *12*, 33751.
[15] C. W. Tseng, H. Y. Chang, J. Y. Chang, C. C. Huang, *Nanoscale* **2012**, *4*, 6823.
[16] Z. Hu, X. Wang, L. Gong, G. Wu, X. Peng, X. Tang, *Inflamm. Res.* **2015**, *64*, 557.
[17] H. S. P. De Souza, C. Fiocchi, *Nat. Rev. Gastroenterol. Hepatol.* **2016**, *13*, 13.
[18] S. Bin Jang, S. M. Jin, H. S. Kim, Y. Y. Jeong, S. J. Lee, S. Hahn, H. Lee, H. S. Lee, J. H. Kim, D. Y. Lee, *Biomaterials* **2022**, *287*, 121679.
[19] J. K. Lee, D. Samanta, H. G. Nam, R. N. Zare, *Nat. Commun.* **2018**, *9*, 11562.
[20] S. Tian, Y. Z. Li, M. B. Li, J. Yuan, J. Yang, Z. Wu, R. Jin, *Nat. Commun.* **2015**, *6*, 8667.
[21] H. S. Kim, M. Seo, T. E. Park, D. Y. Lee, *J. Nanobiotechnol.* **2022**, *20*, 141.
[22] M. J. Mitchell, M. M. Billingsley, R. M. Haley, M. E. Wechsler, N. A. Peppas, R. Langer, *Nat. Rev. Drug Discovery* **2021**, *20*, 101.
[23] P. D. Josephy, T. Eling, R. P. Mason, *J. Biol. Chem.* **1982**, *257*, 3669.
[24] B. Jiang, D. Duan, L. Gao, M. Zhou, K. Fan, Y. Tang, J. Xi, Y. Bi, Z. Tong, G. F. Gao, N. Xie, A. Tang, G. Nie, M. Liang, X. Yan, *Nat. Protoc.* **2018**, *13*, 1506.
[25] C. P. Liu, T. H. Wu, Y. L. Lin, C. Y. Liu, S. Wang, S. Y. Lin, *Small* **2016**, *12*, 4127.
[26] Q. G. J. Malloy, L. Qi, B. Warren, D. R. Cocker, M. E. Erupe, P. J. Silva, *Atmos. Chem. Phys.* **2009**, *9*, 2051.
[27] M. P. Murphy, H. Bayir, V. Belousov, C. J. Chang, K J. A. Davies, M. J. Davies, T. P. Dick, T. Finkel, H. J. Forman, Y. Janssen-Heininger, D. Gems, V. E. Kagan, B. Kalyanaraman, N.-G. Larsson, G. L. Milne, T. Nyström, H. E. Poulsen, R. Radi, H. Van Remmen, P. T. Schumacker, P. J. Thornalley, S. Toyokuni, C. C. Winterbourn, H. Yin, B. Halliwell, *Nat. Metab.* **2022**, *4*, 651.
[28] S. A. Suarez, M. Muñoz, L. Alvarez, M. F. Venâncio, W. R. Rocha, D. E. Bikiel, M. A. Marti, F. Doctorovich, *J. Am. Chem. Soc.* **2017**, *139*, 14483.
[29] H. L. Pu, W. L. Chiang, B. Maiti, Z. X. Liao, Y. C. Ho, M. S. Shim, E. Y. Chuang, Y. Xia, H. W. Sung, *ACS Nano* **2014**, *8*, 1213.
[30] E. Alemany-Cosme, E. Sáez-González, I. Moret, B. Mateos, M. Iborra, P. Nos, J. Sandoval, B. Beltrán, *Antioxidants* **2021**, *10*, 64.
[31] X. Huang, D. He, Z. Pan, G. Luo, J. Deng, *Mater. Today Bio.* **2021**, *11*, 100124.
[32] G. Morris, M. Gevezova, V. Sarafian, M. Maes, *Cell. Mol. Immunol.* **2022**, *19*, 1079.
[33] R. Elmentaite, N. Kumasaka, K. Roberts, A. Fleming, E. Dann, H. W. King, V. Kleshchevnikov, M. Dabrowska, S. Pritchard, L. Bolt, S. F. Vieira, L. Mamanova, N. Huang, F. Perrone, I. Goh Kai'en, S. N. Lisgo, M. Katan, S. Leonard, T. R. W. Oliver, C. E Hook, K. Nayak, L. S. Campos, C. Domínguez Conde, E. Stephenson, J. Engelbert, R. A. Botting, K. Polanski, S. Van Dongen, M. Patel, M. D. Morgan, et al., *Nature* **2021**, *597*, 250.
[34] I. A. Sogias, A. C. Williams, V. V. Khutoryanskiy, *Biomacromolecules* **2008**, *9*, 1837.
[35] J. Schluter, J. U. Peled, B. P. Taylor, K. A. Markey, M. Smith, Y. Taur, R. Niehus, A. Staffas, A. Dai, E. Fontana, L. A. Amoretti, R. J. Wright, S. Morjaria, M. Fenelus, M S. Pessin, N. J. Chao, M. Lew, L. Bohannon, A. Bush, A. D. Sung, T. M. Hohl, M.-A. Perales, M. R. M. Van Den Brink, J. B. Xavier, *Nature* **2020**, *588*, 303.
[36] J. Ni, G. D. Wu, L. Albenberg, V. T. Tomov, *Nat. Rev. Gastroenterol. Hepatol.* **2017**, *14*, 573.
[37] A. Everard, C. Belzer, L. Geurts, J. P. Ouwerkerk, C. Druart, L. B. Bindels, Y. Guiot, M. Derrien, G. G. Muccioli, N. M. Delzenne, W. M. De Vos, P. D. Cani, *Proc. Natl. Acad. Sci. USA* **2013**, *110*, 9066.
[38] C. Maldonado Galdeano, G. Perdigón, *Clin. Vaccine Immunol.* **2006**, *13*, 219.
[39] I. Lagkouvardos, R. Pukall, B. Abt, B. U. Foesel, J. P. Meier-Kolthoff, N. Kumar, A. Bresciani, I. Martínez, S. Just, C. Ziegler, S. Brugiroux, D. Garzetti, M. Wenning, T. P. N. Bui, J. Wang, F. Hugenholtz, C. M. Plugge, D. A. Peterson, M. W. Hornef, J. F. Baines, H. Smidt, J. Walter, K. Kristiansen, H. B. Nielsen, D. Haller, J. Overmann, B. Stecher, T. Clavel, *Nat. Microbiol.* **2016**, *1*, 16131.
[40] J. M. Hoffman, K. G. Margolis, *Nat. Rev. Gastroenterol. Hepatol.* **2020**, *17*, 6.
[41] H. Liu, Z. Cai, F. Wang, L. Hong, L. Deng, J. Zhong, Z. Wang, W. Cui, *Adv. Sci.* **2021**, *8*, 21016191.
[42] C. Shi, J. Dawulieti, F. Shi, C. Yang, Q. Qin, T. Shi, L. Wang, H. Hu, M. Sun, L. Ren, F. Chen, Y. Zhao, F. Liu, M. Li, L. Mu, D. Liu, D. Shao, K. W. Leong, J. She, *Sci. Adv.* **2022**, *8*, eabj2372.
[43] S. Zhao, Y. Li, Q. Liu, S. Li, Y. Cheng, C. Cheng, Z. Sun, Y. Du, C. J. Butch, H. Wei, *Adv. Funct. Mater.* **2020**, *30*, 2004692.
[44] U. Barayeu, D. Schilling, M. Eid, T. N. Xavier Da Silva, L. Schlicker, N. Mitreska, C. Zapp, F. Gräter, A. K. Miller, R. Kappl, A. Schulze, J. P. Friedmann Angeli, T P. Dick, *Nat. Chem. Biol.* **2023**, *19*, 28.
[45] H. E. Harris, U. Andersson, D. S. Pisetsky, *Nat. Rev. Rheumatol.* **2012**, *8*, 195.
[46] R. K. Boyapati, A. G. Rossi, J. Satsangi, G. T. Ho, *Mucosal Immunol.* **2016**, *9*, 567.
[47] P. Scaffidi, T. Misteli, M. E. Bianchi, *Nature* **2002**, *418*, 191.
[48] S. Vermeire, G. Van Assche, P. Rutgeerts, *Nat. Clin. Pract. Gastroenterol. Hepatol.* **2005**, *2*, 580.
[49] I. Cho, M. J. Blaser, *Nat. Rev. Genet.* **2012**, *13*, 260.
[50] S. V. Lynch, O. Pedersen, *N. Engl. J. Med.* **2016**, *375*, 2369.
[51] M. Snelson, C. de Pasquale, E. I. Ekinci, M. T. Coughlan, *Best. Pract. Res. Clin. Endocrinol. Metab.* **2021**, *35*, 101507.
[52] J. Zhou, M. Li, Q. Chen, X. Li, L. Chen, Z. Dong, W. Zhu, Y. Yang, Z. Liu, Q. Chen, *Nat. Commun.* **2022**, *13*, 3432.
[53] J. Li, R. Cha, X. Zhao, H. Guo, H. Luo, M. Wang, F. Zhou, X. Jiang, *ACS Nano* **2019**, *13*, 5002.
[54] J. Lloyd-Price, C. Arze, A. N. Ananthakrishnan, M. Schirmer, J. Avila-Pacheco, T. W. Poon, E. Andrews, N. J. Ajami, K. S. Bonham, C. J. Brislawn, D. Casero, H. Courtney, A. Gonzalez, T. G. Graeber, A. B Hall, K. Lake, C. J. Landers, H. Mallick, D. R. Plichta, M. Prasad, G. Rahnavard, J. Sauk, D. Shungin, Y. Vázquez-Baeza, R. A. White, J. Braun, L. A. Denson, J. K. Jansson, R. Knight, S. Kugathasan, et al., *Nature* **2019**, *569*, 655.